Nano Energy 33 (2017) 453–461

Contents lists available at ScienceDirect

Nano Energy

journal homepage: www.elsevier.com/locate/nanoen

Full paper

# Optimized mesopores enabling enhanced rate performance in novel ultrahigh surface area meso-/microporous carbon for supercapacitors

Jie Yang[1], Haolin Wu[1], Min Zhu, Wenju Ren, Yuan Lin, Haibiao Chen*, Feng Pan*

*School of Advanced Materials, Peking University, Shenzhen Graduate School, Shenzhen 518055, People's Republic of China*

ARTICLE INFO

*Keywords:*
Mesoporous carbon
*In-situ* template
Polysiloxane
Supercapacitors
High energy density

ABSTRACT

Increasing both the energy density and the power density of supercapacitors is an important but challenging research subject. Porous carbon with extremely high surface, such as activated carbon, is a key engineering material for current supercapacitor technology. Here we report optimized mesopores enabling significantly enhanced rate performance in hierarchically meso-/microporous carbon with a ultrahigh surface area for supercapacitors, which is prepared by a new *in-situ* template method to exhibit a high mesopore volume proportion (66.0%), as well as a large pore volume up to 2.47 $cm^3 g^{-1}$, and an ultrahigh specific surface area of 3122 $m^2 g^{-1}$. Polysiloxane was used as a precursor to produce nonporous SiOC, and sequentially NaOH was used to activate SiOC to produce highly porous carbon by removing silica and activating carbon. Hierarchically porous carbon C800 exhibited a high energy density up to 42 Wh $kg^{-1}$ at a power density of 374 W $kg^{-1}$, and still retained an energy density of 21 Wh $kg^{-1}$ at a high power density of 30 kW $kg^{-1}$. The superior rate performance of the supercapacitor is attributed to that C800 contains a majority proportion of mesopores which facilitate fast ion migration during high power charging/discharging.

## 1. Introduction

Electricity generated from renewable resources such as solar energy, hydropower, and biofuels is envisioned to power a greener and more sustainable future. Rechargeable batteries, especially Li-ion batteries, are one of the most important energy storage devices enabling on-site utilization of the electrical energy. Supplemental to rechargeable batteries, supercapacitors fill the gap on the energy storage scheme with exceptional power density [1,2]. In general, supercapacitors can be classified into two categories: electrical double-layer capacitors (EDLCs) based on charge storage at the electrode/electrolyte interface and pseudocapacitors through reversible redox reactions [1–3]. EDLCs based on porous carbons have recently attracted tremendous attention due to the high power density and almost unlimited cycle life [4,5]. However, the much low energy densities (approximately 5 Wh $kg^{-1}$) of commercial EDLCs have hindered their wide applications [6–9]. Owing to its super high surface area and electrical conductivity, porous carbon is an ideal material for EDLCs. Generally, the performance of carbon materials in EDLCs is highly dependent on the migration and adsorption of ions inside nanopores, which are largely determined by the pore structure of the material [10–12].

Traditionally, activated carbons have been the choice of the electrode material in EDLCs. Activated carbons are produced by either physical or chemical activation of carbon rich precursors [13–22]. Typical activated carbon materials are predominantly microporous (pore width $< 2$ nm) and the specific surface area can exceed 3000 $m^2 g^{-1}$. However, micropores are not easily accessible to large ions when the electrolyte is organic or ionic liquid, which can work at a higher operating voltage with a higher energy density but a lower power density due to slower mass transfer [23–32]. Introducing mesopores (pore width of 2–50 nm) to porous carbon can improve effective utilization of the pore surface area and accelerate mass transfer so as to enhance the power density. Usually increasing the pore size leads to the reduction of the specific surface area if the specific pore volume remains constant. To optimize porous carbon materials for maximum effective surface area, both the specific surface area and the specific pore volume will need to be increased simultaneously [33].

One approach to produce mesoporous carbon is to use unconventional precursors with the conventional activation process. Recently, activated graphene synthesized by KOH activation following microwave expansion was found to be highly mesoporous with a specific surface area exceeding 3000 $m^2 g^{-1}$ [8,34]. Another approach to introduce pores with controlled pore size distribution is to integrate sacrificial *ex-*

* Corresponding authors.
*E-mail addresses:* chenhb@pkusz.edu.cn (H. Chen), panfeng@pkusz.edu.cn (F. Pan).
[1] These authors contributed equally to this work.

http://dx.doi.org/10.1016/j.nanoen.2017.02.007
Received 28 December 2016; Received in revised form 24 January 2017; Accepted 6 February 2017
Available online 08 February 2017

*situ* or *in-situ* templates into the carbon precursors [35,36]. However, using an *ex-situ* sacrificial template complicates the process and increases the materials cost. Alternatively, porous carbon can be produced from carbon-forming alloys or ceramics with a homogeneous nanostructure by selectively removing the non-carbon phases. Gogotsi's group produced carbide derived carbons (CDCs) using a chlorination process with precise control of the pore size, and successfully applied the materials for supercapacitors [24,25,30] and hydrogen and methane storage [37]. Pena-Alonso et al. showed that silicon oxycarbide (SiOC) ceramics can be etched by hydrofluoric (HF) acid to form porous carbon materials with specific surface area up to 600 $m^2 g^{-1}$ [38]. In these methods, toxic chemicals were used to etch the carbon precursor to produce pores, which will be a concern for large scale production.

In this article we report a new class of hierarchically meso-/microporous carbon materials produced from polysiloxane precursors using a simple alkaline activation process. Polysiloxanes have long been used as precursors to produce SiOC ceramics. Upon pyrolysis of polysiloxane, silica and carbon atoms rearrange and phase segregate into a homogenous nanoscale structure containing silica nanodomains dispersed in a graphene network [39]. Selectively removing one phase will create pores in the structure, as demonstrated by Gogotsi's group [40,41] and Pena-Alonso et al [38]. We extend the concept by using SiOC to produce carbon materials with very high surface area employing an alkaline activation process, and especially introducing a very large mesopore volume. In comparison to mainly micropores in traditional activated carbon, the optimized mesopores in the hierarchically porous carbon in this work achieved both maximum effective surface area and fast mass transfer, by bridging the micropores and the external environment. The value of this carbon material with unique pore structure and properties was demonstrated in EDLC application. The EDLCs employing the polysiloxane-derived carbon showed a high specific capacitance and excellent rate performance, demonstrating both high energy density and power density.

## 2. Material and methods

### 2.1. Synthesis of polysiloxane-derived carbon

The synthesis of polysiloxane-derived carbon is schematically illustrated in Scheme 1. Polysiloxane elastomer was prepared by addition-polymerization of vinyl-terminated phenyl-methyl polysiloxane using polymethylhydrosiloxane (PMHS) as a cross-linker. The purpose of selecting phenyl-rich precursor was to obtain a high carbon content and improve the product yield. In a typical procedure, 20 g of vinyl-terminated phenol-methyl polysiloxane (UC252, viscosity 3000 mPa s, Jiaxing United Chemistry, China) and 1 g of PMHS (Sigma-Aldrich) were reacted with the addition of 15 μL 2 wt% Pt catalyst solution (platinum(0)-1,3-divinyl-1,1,3,3-tetramethyldisiloxane complex solution in xylene, Sigma-Aldrich) at room temperature. The cross-linked polymer was pyrolyzed in a tube furnace (MTI Corporation) under argon flow. The furnace was heated from room temperature to 1200 °C at 10 °C/min ramp rate and hold at 1200 °C for one hour before cooling down to room temperature at 10 °C/min ramp rate. The polymer-ceramic conversion was accompanied by 44% weight loss (Fig. S2) due to loss of hydrogen, volatile hydrocarbons, and silanes. The resulted SiOC ceramic was designated as SiOC1200. The bulk composition of SiOC1200 can be described as $SiO_{0.9}C_{2.2}$ according to elemental analysis [42]. SiOC1200 was pulverized and mixed with NaOH particles in a ratio of 1:4. The mixture was placed in a nickel boat and heated in a tube furnace to a temperature in the range of 400–900 °C at 5 °C/min ramp rate and hold at that temperature for one hour before cooling down at 5 °C/min ramp rate under argon flow. The heat treatment temperature was selected within a range from 400 through 900 °C at 100 °C intervals and the products were labeled as C400 through C900 accordingly. At above 400 °C, the molten NaOH is expected to etch the silica phase according to [43,44]:

$$2NaOH + SiO_2 \rightarrow Na_2SiO_3 + H_2O \quad (1)$$

Meanwhile, carbon was attacked by NaOH which is commonly known as the "activation" process. When the activation temperature was in the lower range (e.g. below 750 °C), it is believed that the activation reaction can be described by the following equation [43]:

$$4NaOH + C \rightarrow Na_2CO_3 + Na_2O + 2H_2 \quad (2)$$

When the activation temperature is above 750 °C, the activation reaction can be described by the following equation [45,46]:

$$6NaOH + 2C \rightarrow 2Na_2CO_3 + 2Na + 3H_2 \quad (3)$$

The product was washed with copious amount of de-ionized water. The washing continued until the filtrate water became neutral in pH value. Carbon particles were collected and dried in a vacuum oven at 120 °C. During the washing step, sodium silicate and sodium carbonate were leached out and a hierarchically porous carbon material was obtained. Thermogravimetric analysis (TGA) in oxygen showed nearly 100% weight loss (Fig. S2), demonstrating the high purity of the as-prepared carbon materials. For comparison, another sample was prepared by etching SiOC1200 using HF acid at room temperature. Since HF is not supposed to attack carbon, only silica was removed to form pores. Additionally, a commercial activated carbon YP50 (Kuraray Chemical) was used for comparison with in-house materials.

### 2.2. Materials characterization

To characterize the pore structure of the carbon materials, nitrogen physisorption analysis was carried out on a Micromeritics ASAP 2020

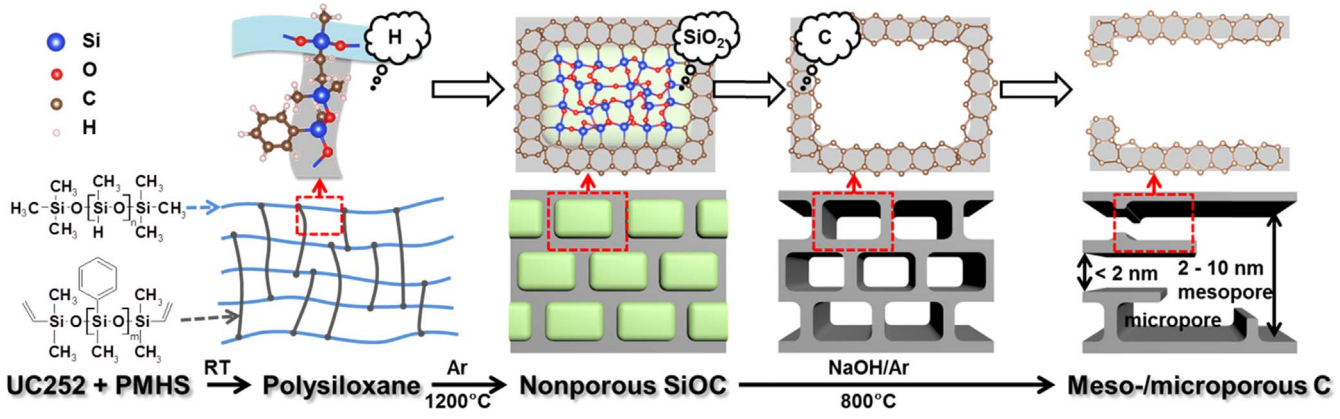


**Scheme 1.** Synthesis of highly mesoporous carbon from polysiloxane via NaOH etching and activation.

unit. The surface area was calculated using the Brunauer-Emmett-Teller (BET) model and pore size distribution (PSD) was derived by a density functional theory (DFT) model based on the nitrogen adsorption data. The morphology was observed with scanning electron microscopy (SEM, ZEISS Supra 55) and transmission electron microscopy (TEM, FEI Tecnai G2 F30). The phase composition was analyzed by X-ray diffraction (XRD) using a Bruker D8 Advance diffractometer with Cu-Kα radiation. Raman spectra were collected using a Horiba modular Raman system containing an Olympus BX41 microscopy, a diode laser source (wave length 532 nm, LEO Photoelectric Co., Ltd, China), a Horiba iHR320 spectrometer, and a Synapse CCD detector. X-ray photoelectron spectra (XPS) were obtained using an ESCALAB 250XL X-ray photoelectron spectrometer.

### 2.3. Electrochemical test

Typically, the working electrode was made of active material, conductive agent (acetylene black), and polymer binder (polytetrafluoroethylene, PTFE) in a mass ratio of 8:1:1, respectively. All the above components were mixed well and ground into a paste in a mortar with addition of isopropyl alcohol. Then the paste was rolled into uniformly thin sheets (thicknesses from 100 to 150 μm) and punched into 1 cm diameter plates. The plates were dried at 120 °C for 12 h under vacuum to remove solvent, and pressed onto nickel foam to produce the work electrode. The mass loading of the active materials varied from 2 to 2.5 mg $cm^{-2}$. The three-electrode tests were performed in the electrolyte of 6.0 M KOH with Hg/HgO electrode as the reference electrode and Pt plate as the counter electrode. For two-electrode test, a CR2032 coin-cell type device was assembled using a pair of circular electrode plates sandwiching a Whatman separator and 1 M tetraethylammonium tetrafluoroborate/acetonitrile ($TEABF_4$/AN) solution as the electrolyte. The cyclic voltammetry (CV) measurement and electrochemical impedance spectroscopy (EIS) test were carried out on a CHI660 electrochemical workstation (Shanghai Chenhua Instrument Co., Ltd.). The EIS data were obtained at open circuit voltage with an AC amplitude of 5 mV in the frequency range of 0.01 Hz–100 kHz. The charging/discharging tests were performed on a Maccor MC16 high precision battery testing system. All the electrochemical tests were carried out at room temperature.

Based on the discharging curves, the specific capacitance ($C_s$) for was calculated according to the following equation:

$$C_s = \frac{I\Delta t}{m\Delta V} \tag{4}$$

where $I$ (A) is the current, $\Delta V$ (V) is the discharging potential change minus the IR drop and $\Delta t$ (s) is the discharging time corresponding to $\Delta V$. $m$ (g) represents the mass of the active material in a single carbon electrode.

The energy density E (Wh $kg^{-1}$) and power density P (W $kg^{-1}$) were calculated from the following equations:

$$E = \frac{1}{2}C(\Delta V)^2 \tag{5}$$

$$P = \frac{E}{\Delta t} \tag{6}$$

where C (F $g^{-1}$) is the gravimetric capacitance, $\Delta V$ (V) is operating potential, and $\Delta t$ (h) is the discharging time.

## 3. Results and discussion

### 3.1. Structural features

The nitrogen adsorption/desorption isotherms of the samples are shown in Fig. 1**a**, and the corresponding DFT pore size distributions are shown in Fig. 1**b**. The isotherms of C400 and HF-etched sample can be classified as type I isotherm, which corresponds to microporous materials, since majority of the nitrogen adsorption takes place at very low pressure range ($P/P_0 < 0.05$) via micropore filling. With the temperature increasing to 700 °C and 800 °C, the adsorption volumes dramatically increase and the isotherms show obvious features of type IV isotherm. The significant hysteresis loop in the isotherm suggests that there are mesopores existing in C700 and C800. The isotherm of sample C900 displays the same feature as that of the C800, but the adsorption volume begins to decrease. For quantitative analysis, the specific surface area was derived using the BET method and the specific pore volume was obtained by taking the adsorption volume at relative pressure close to unity, shown in Table S1. It is noted that the BET specific surface area of C800 reaches a maximum of 3122 $m^2 g^{-1}$ with a specific pore volume of 2.47 $cm^3 g^{-1}$. In addition, it has the highest volume proportion of mesopores at 66.0% among all the samples. The BET specific surface area, specific pore volume, and mesopore volume of C800 are all among the highest values for porous carbon materials recently reported as shown in Table S2.

The PSD shown in Fig. 1**b** suggests that both the micropore volume and the mesopore volume increase as the activation temperature increases within the range of 400–800 °C, and decrease at 900 °C. During activation, the temperature is a vital factor impacting the formation of pore structure and the value of the specific surface area. Based on the variation of PSD according to the temperature, a possible mechanism for the formation of pore structure is proposed. Compared to the process of HF-etching, more pores were created during NaOH activation due to the etching of both silica and carbon. When the activation temperature was relatively low such as 400 °C and 500 °C, the removal of silica played a dominant role without etching much carbon so that majority of the created pores were in the range of micropore. This can be confirmed by the result that the average pore sizes of C400 and C500 are similar to the size of the initial silica nanodomains in SiOC [42]. At a relatively high temperature of 800 °C, the adjacent pores previously created due to silica removal were connected as the carbon walls were broken down, leading to the formation of a large number of mesopores. Also new pores were likely created on the carbon walls, which is similar to the activation mechanism of most porous carbon materials. When the activation temperature further increased to 900 °C, the BET specific surface area dropped drastically to 1646 $m^2 g^{-1}$ and the pore volume dropped to 1.33 $cm^3 g^{-1}$, probably because the pore structure partial collapsed causing reduction in pore volume and surface area. It is noted that the carbon skeleton tend to be excessively etched at a higher temperature. Also, a higher temperature facilitates the reorganization and restacking of graphene sheets, causing the elimination of inter-layer pores.

The XRD spectra of the samples are shown in Fig. 2**a**. The XRD spectrum of SiOC1200 shows a peak at around 26.6°, corresponding to the (002) planes of graphite. The (101) peak near 44° is very broad and weak, suggesting misalignment between the graphene layers and a low degree of graphitization. Similar peaks are found for sample C400, although the (002) peak significantly broaden and shifts to a lower angle at around 23°. Shifting of the (002) peak corresponds to a change of the graphene layer spacing from 0.335 to 0.384 nm [42]. Likely NaOH activation caused the expansion of the layered structure, especially after the space-filling silica phase was removed. In the XRD pattern of C800, the (002) peak almost disappears and only a broad (101) peak is visible. When activated at 800 °C, carbon started to lose its ordered structure as it became highly porous due to vigorous NaOH etching [34]. The (002) peak reappears in the XRD pattern of C900, suggesting reconstruction of the structure takes place at this temperature. Inevitably, crystallization of the structure leads to elimination of pores and reduction of the specific surface area, as previously shown in the physisorption measurement. The Raman spectra of the materials are shown in Fig. 2**b**. The D band near 1340 $cm^{-1}$ originates from the 6-fold ring breathing mode vibration, which is only possible at free edges. G band near 1580 $cm^{-1}$ originates from the in-plane stretching mode vibration. The ratio of the intensity of D band to the

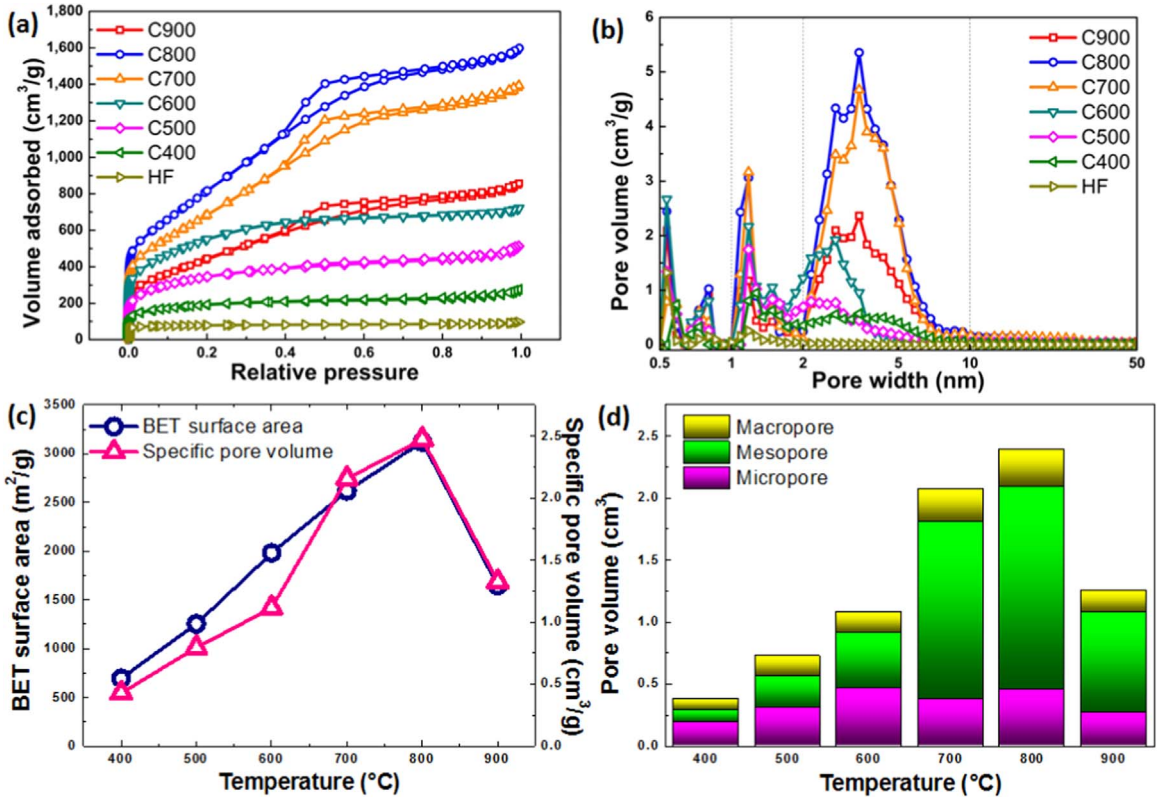


**Fig. 1.** (a) Nitrogen physisorption isotherms of polysiloxane-derived carbon; (b) DFT pore size distribution; (c) BET specific surface area and specific pore volume vs. activation temperature; (d) Composition of macropores, mesopores, and micropores vs. activation temperature.

intensity of G band ($I_D/I_G$) is commonly used to estimate the defect population or crystallite size of carbon materials [47,48]. The $I_D/I_G$ values of SiOC1200, C400, C500, C600, C700, C800, and C900 are 1.16, 0.84, 0.91, 1.01, 1.10, 1.08, and 1.09, respectively. The Raman result suggests that carbon in SiOC1200 has the highest density of free edges, or defects, although SiOC1200 is not porous at all. After removal of the silica phase, the graphene layers appeared to reorganize and the number of defects decreased, although pores were being created at the same time. As the activation temperature increased, both reorganization and attacking of carbon became more significant, with the former eliminates defects while the latter produced defects. More reorganization took place during the formation of C900, with 2D peak appears as an indication of stacking of several graphene layers.

The surface compositions of C800 as investigated by XPS are shown in Fig. 2**c** and **d**. The XPS analysis reveals that the samples are mainly composed of C (ca. 89.14 wt%) and O (ca.9.84 wt%) with a small amount of Si (ca.1.02 wt%), which is in good agreement with the TGA result. The high-resolution C1s spectrum can be deconvoluted into three peaks assigned to the C-C/C=C bond (~284.8 eV), C-O (~285.5 eV), and C=O (~288.9 eV), respectively [49–51]. The high-resolution O1s spectrum can be fitted to two peaks corresponding to C=O (531.6 eV) and C=O (532.9 eV) [52,53]. The abundant presence of O functional groups in the prepared materials can facilitate the wettability of the electrode, leading to an effective mass transfer.

The morphology of the polysiloxane-derived carbon materials as observed by SEM and TEM are shown in Fig. 2**e** and **f**. SiOC1200 appears to have a nonporous morphology under SEM. Fig. 2**f** displays a sponge-like morphology of C800 with abundant nano/micropores. The corresponding inset of TEM further reveals that several layers of graphitized carbon form the twisted crystalline domains containing lots of defects [22].

### 3.2. Electrochemical performance

In the three-electrode tests, the specific capacitance was found to be almost proportional to the specific surface area, and the area-normalized specific capacitance was around 10 μF $cm^{-1}$ (Figs. S5 and S6). C800 demonstrated the highest specific capacitance and superior rate performance owing to its highest specific surface area and a large volume of mesopores among all samples. The cyclic voltammetry (CV) measurement of C800 performed using various scan rates from 5 to 200 mV/s in voltage range of −1.0 to 0 V is shown in Fig. 3**a**. The CV curves show a quasi-rectangular shape at different scanning rates, indicting a typical characteristic of double-layer capacitor behavior and a superior rate capability. The EDLC was further tested at various charging/discharging current densities, shown in Fig. 3**b**. The charging/discharging curves are close to symmetric triangle and show a very small voltage drop, suggesting a low resistance and the efficient double-layer charge storage. The specific capacitance of the materials was calculated from the charging/discharging measurements. As shown in Fig. 3**e**, a high specific capacitance of 327 F $g^{-1}$ is achieved at a current density of 0.5 A $g^{-1}$. Even at an ultrahigh current density of 50 A $g^{-1}$, the specific capacitance is still as high as 198 F $g^{-1}$, which is among the best reported performances based on carbon materials [1,54–57]. The cycling stability of the EDLC was tested at 5 A $g^{-1}$ for 10,000 cycles. After 10,000 cycles, the capacitance retention is still as high as 93.9%, showing that the material has excellent stability.

These results suggest that the beneficially hierarchical pore layout of C800 can facilitate fast ion response and charge transfer, leading to a superior rate performance, which is further revealed by electrochemical impedance spectroscopy (EIS) in Fig. S8. The Nyquist plot indicates that the C800 shows a nearly ideal capacitive behavior with a small equivalent series resistance of 0.40 Ω, which contains the resistance of

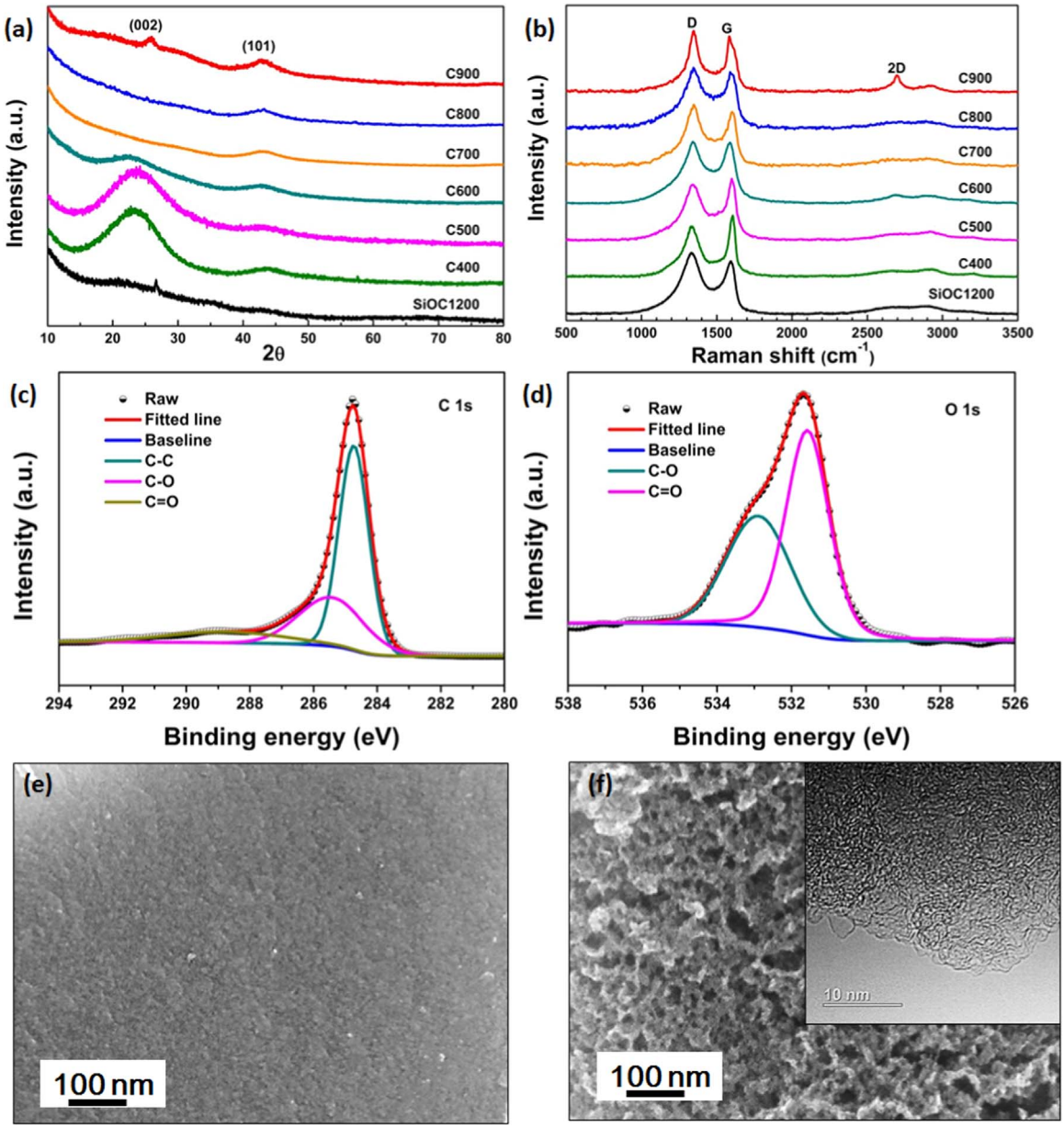


**Fig. 2.** (a) XRD of SiOC-1200, C400-C900; (b) Raman spectra of SiOC-1200, C400-C900; (c) High resolution C 1s XPS spectrum of C800; (d) High resolution O 1s spectrum of C800; (e) SEM of SiOC-1200; (f) SEM of C800 and TEM of C800 (inset).

the active material, the resistance of the electrolyte and contact resistance at the interface. In the high-frequency region, the small semicircle with a diameter of 0.89 Ω means a low charge-transfer resistance in the active material. A nearly vertical slope at the low-frequency region reveals the excellent pore accessibility for the electrolyte and fast ion response [9,57,58].

In the two-electrode test in symmetrical EDLCs with $TEABF_4$/AN electrolyte, the CV was measured in a voltage range of 0–2.5 V using various scan rates as shown Fig. 3**c**. The CV curves are also close to rectangular shapes, suggesting a typical EDLC behavior. Meanwhile, charging/discharging curves (shown in Fig. 3**d**) display a highly symmetric triangular shape, indicating an excellent EDLC behavior. As shown in Fig. 3**e**, the specific capacitance is 163 F $g^{-1}$ at a current density of 0.5 A $g^{-1}$, and it gradually decreases as the current density increases. At a current density of 50 A $g^{-1}$, the specific capacitance is about 129 F $g^{-1}$. The cycle performance of the EDLC in the organic electrolyte was measured at 2 A $g^{-1}$ for 10,000 cycles. At the end of the test, the capacity retention was at 90.3%.

The performance of C800 is compared to YP50 as shown in Figs. S9 and S10. YP50 is also a meso-/microporous material but with a lower specific surface area and a lower mesopore volume proportion (See Table S1 and Fig. S3). In the organic electrolyte, C800 showed much higher gravimetric specific capacitance and also higher capacitance retention in comparison to YP50. The result suggests that a large mesopore volume is essential in facilitating ion transport within the porous electrode material. The fitting EIS data in Fig. S8 show that the equivalent series resistance (ESR) and the charge-transfer resistance of YP50 are 0.51 Ω and 1.10 Ω, respectively, which are both higher than those of C800, suggesting that there is a lower diffusion resistance and charge-transfer resistance in C800. To further increase the energy density, the voltage was increased to 3 V, shown in Fig. S10 and S11, C800 continued to demonstrate excellent capacitance retention even at this high voltage. A Ragone plot was generated for these materials and shown in Fig. 4**a**. C800 shows a maximum energy density of 31 Wh $kg^{-1}$ at a power density of 311 W $kg^{-1}$ when tested at 2.5 V, and a maximum energy density of 42 Wh $kg^{-1}$ at a power density of

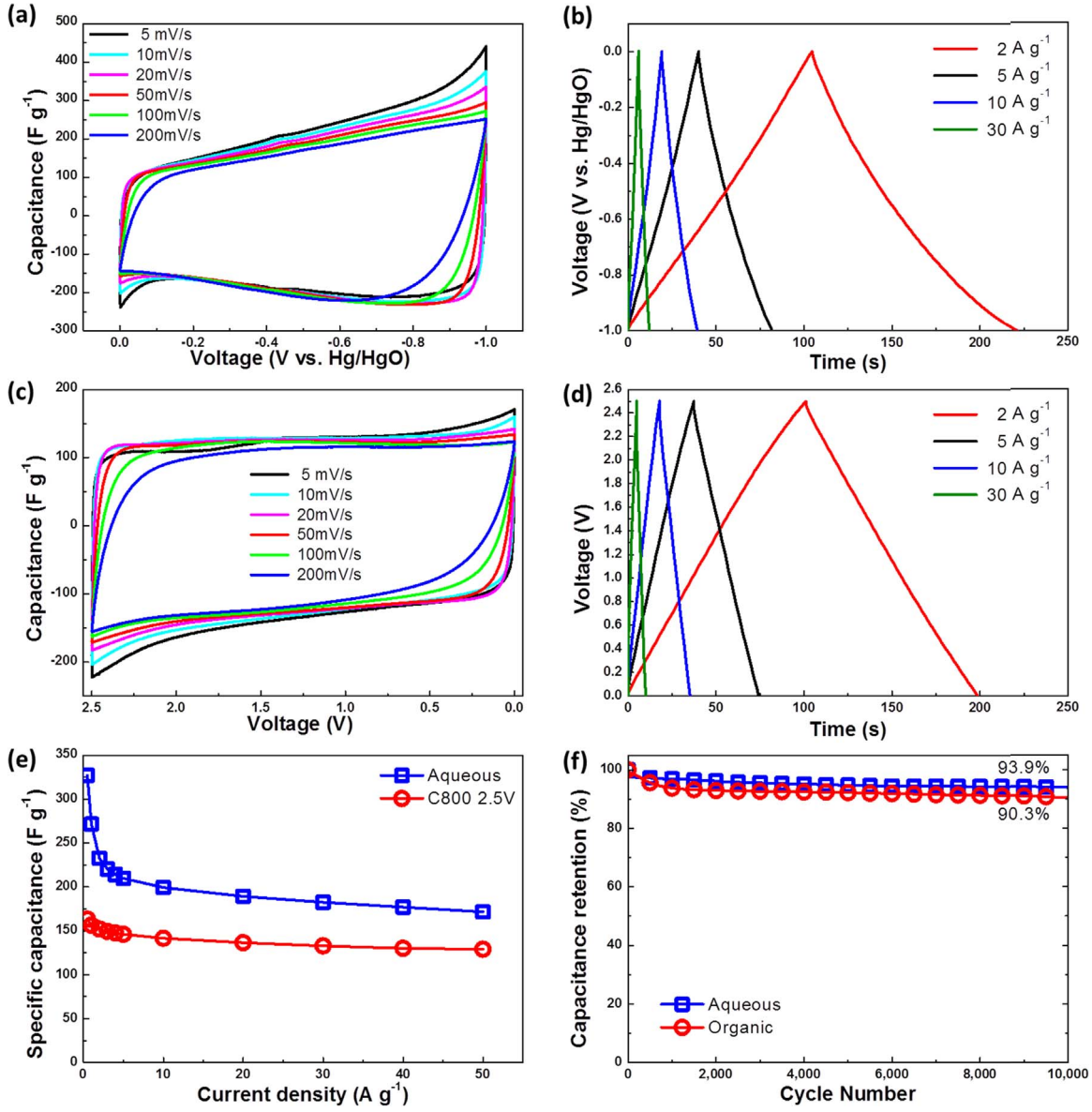


**Fig. 3.** EDLC performance of C800 tested in 6 M KOH electrolyte using a three-electrode configuration: (a) cyclic voltammetry at various scan rates; (b) galvanostatic charging/discharging curves at different current densities; EDLC performance of C800 tested in 1 M $TEABF_4$/AN electrolyte using a two-electrode configuration: (c) cyclic voltammetry at various scan rates; (d) galvanostatic charging/discharging curves at different current densities; (e) Specific capacitance as a function of current density in aqueous and organic electrolytes; (f) Cycling stability at a current density of 5 A $g^{-1}$ in aqueous and organic electrolytes.

372 W $kg^{-1}$ when tested at 3 V. C800 retains an energy density of 21 Wh $kg^{-1}$ even at a high power density of 30 kW $kg^{-1}$ when tested at 3 V. The energy density is one order of magnitude higher than that of commercial EDLCs, without losing the power capability. The performance of C800 is competitive when compared to the best values recently reported for carbon materials used in EDLCs with comparable voltage range [10,18,22,50,52,54,59–70]. Therefore, a high specific surface area combined with a high mesopore volume proportion is essential for a porous carbon material used in EDLCs for achieving superior performance.

We propose a qualitative model of ion migration to explain why the hierarchically meso-/microporous carbon material with optimized mesopores enables to perform ultrahigh rate capability, in contrast why a solely microporous carbon material to perform lower rate capability. In a solely microporous carbon material, the average pore width is not much larger than the diameter of the solvated ions of tetraethylammonium ($TEA^+$) or tetrafluoroborate ($BF_4^-$). As shown on the left of Fig. 4**b**, typical porous carbon material contains high aspect-ratio slit-type pores which are deep and narrow. During charging/discharging, counter-ions migrate towards/away from the charged surface through these deep-and-narrow micropores at a limited velocity. At a high charging/discharging rate, the migration of counter-ions in the micropores lags behind the charge flow in/out of the electrode, leading to reduction of the capacitance. Also, the micropores tend to trap co-ions inside the pores, causing the reduction of the net charge density and the capacitance [71]. In contrast, when mesopores are created by connecting neighboring micropores as shown on the right of Fig. 4**b**, the depth of the micropores is greatly reduced. Ions migrating within this meso-/microporous structure experience much lower resistance and can travel from/to the charged surface quickly. Also, the possibility of co-ions being trapped inside shallow micropores or mesopores is much reduced. Therefore, the capacitance in this

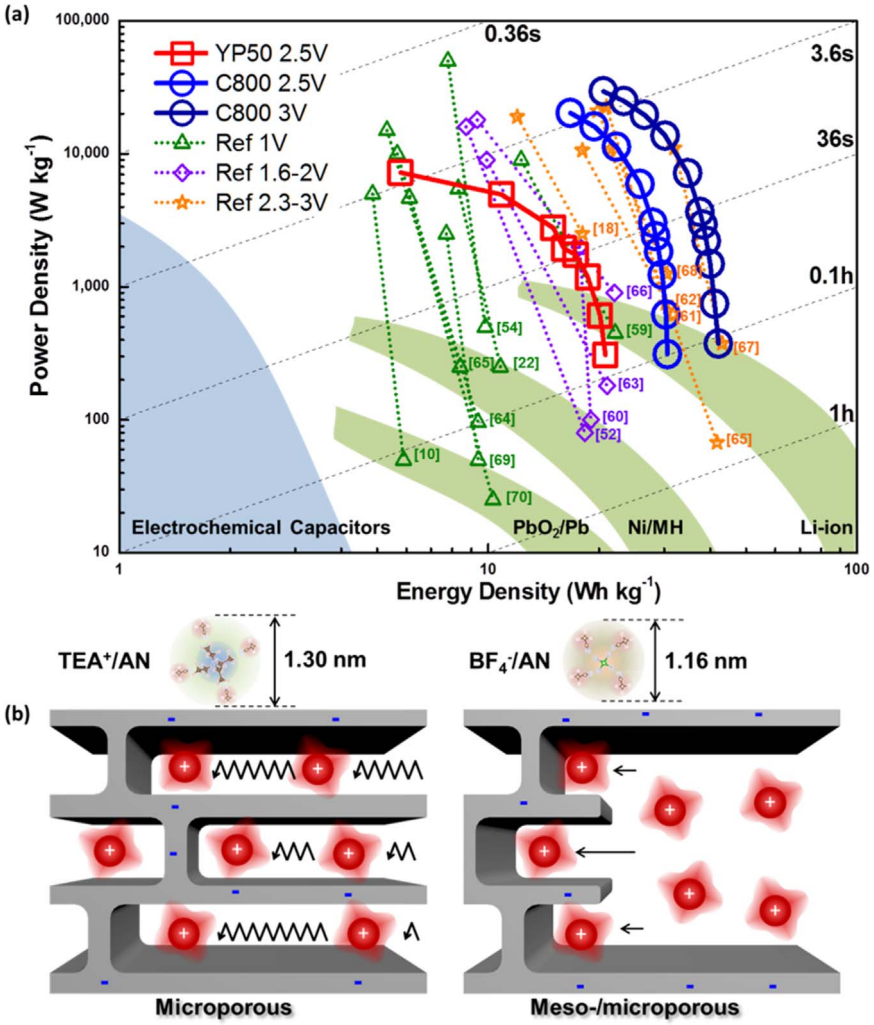


**Fig. 4.** (a) Ragone plot of C800 and commercial YP50 as supercapacitor electrodes in organic electrolyte, in comparison to recently reported values (Note: Only values from EDLCs, i.e., no major contribution from pseudocapacitance, with a voltage window no wider than 3 V were selected from the literature); (b) Comparison of ion transport in microporous and meso-/microporous materials.

meso-/microporous structure can be retained even at a very high charging/discharging rate. Both a high energy density and a high power density can be achieved simultaneously with the meso-/microporous structure proposed.

## 4. Conclusions

In summary, we develop a new class of polysiloxane-derived carbon materials with a large mesopore volume and a very high surface area contributed by its hierarchal meso-/microporosity. Different from conventional activated carbon materials with a high specific surface area but mostly micropores, polysiloxane-derived carbon materials contain mostly mesopores. The silica nanodomains in the SiOC ceramic derived from pyrolysis of polysiloxane play as an *in-situ* template to form mesopores in the final carbon product. Potentially, the pore structure of the final carbon product can be tuned by tailoring the formula of the polysiloxane precursor. The hierarchal meso-/microporosity facilitates fast transport of molecules and ions between the internal surface and outside environment, maximizing the effective surface area of the material in various applications. Owing to its mesoporosity, polysiloxane-derived carbon displayed superior rate performance in EDLCs with an organic electrolyte. The specific capacitance at a current density of 50 A $g^{-1}$ was 80% of the specific capacitance at a current density of 0.5 A $g^{-1}$. The polysiloxane-derived carbon achieved a maximum energy density of 42 Wh $kg^{-1}$ and a maximum power density of 30 kW $kg^{-1}$, which were significantly higher than those of the commercial YP50 activated carbon.

In addition, we verified that the NaOH activation process can be extended to other polysiloxane materials. Using a similar processing protocol, carbon with the same high specific surface area and high mesopore volume was prepared from a single-component polysiloxane. We anticipate that this class of polysiloxane-derived carbon material will be a promising addition to the porous carbon materials family to further enhance the materials performance in many applications.

## Acknowledgements

This research was financially supported by the National Materials Genome Project (2016YFB0700600), the Guangdong Innovation Team Project (No. 2013N080), and the Shenzhen Science and Technology Research Grants (No. JCYJ20150626110958181, JCYJ20150518092933435).

## Appendix A. Supporting information

Supplementary data associated with this article can be found in the online version at doi:10.1016/j.nanoen.2017.02.007.

## References


[1] J. Yan, Q. Wang, T. Wei, Z. Fan, Recent advances in design and fabrication of electrochemical supercapacitors with high energy densities, Adv. Energy Mater. (2014) 1300816.
[2] A. Burke, Ultracapacitors: why, how, and where is the technology, J. Power Sources 91 (2000) 37–50.
[3] M.D. Stoller, S. Park, Y. Zhu, J. An, R.S. Ruoff, Graphene-based ultracapacitors, Nano Lett. 8 (2008) 3498–3502.
[4] A.G. Pandolfo, A.F. Hollenkamp, Carbon properties and their role in supercapacitors, J. Power Sources 157 (2006) 11–27.
[5] M. Wang, X. Song, S. Dai, W. Xu, Q. Yang, J. Liu, C. Hu, D. Wei, NiO nanoparticles supported on graphene 3D network current collector for high-performance electrochemical energy storage, Electrochim. Acta 214 (2016) 68–75.
[6] A. Burke, R & D considerations for the performance and application of electrochemical capacitors, Electrochim. Acta 53 (2007) 1083–1091.
[7] Y. Jin, K. Tian, L. Wei, X. Zhang, X. Guo, Hierarchical porous microspheres of activated carbon with a high surface area from spores for electrochemical double-layer capacitors, J. Mater. Chem. A (2016).
[8] T. Kim, G. Jung, S. Yoo, K.S. Suh, R.S. Ruoff, Activated graphene-based carbons as supercapacitor electrodes with macro- and mesopores, ACS Nano 7 (2013) 6899–6905.
[9] J. Xu, Z. Tan, W. Zeng, G. Chen, S. Wu, Y. Zhao, K. Ni, Z. Tao, M. Ikram, H. Ji, Y. Zhu, A hierarchical carbon derived from sponge-templated activation of graphene oxide for high-performance supercapacitor electrodes, Adv. Mater. 28 (2016) 5222–5228.
[10] Y. Gong, Z. Wei, J. Wang, P. Zhang, H. Li, Y. Wang, Design and fabrication of hierarchically porous carbon with a template-free method, Sci. Rep. 4 (2014) 6349.
[11] Q. Li, R. Jiang, Y. Dou, Z. Wu, T. Huang, D. Feng, J. Yang, A. Yu, D. Zhao, Synthesis of mesoporous carbon spheres with a hierarchical pore structure for the electrochemical double-layer capacitor, Carbon 49 (2011) 1248–1257.
[12] J. Wei, D. Zhou, Z. Sun, Y. Deng, Y. Xia, D. Zhao, A controllable synthesis of rich nitrogen-doped ordered mesoporous carbon for CO2 capture and supercapacitors, Adv. Funct. Mater. 23 (2013) 2322–2328.
[13] M.S. Balathanigaimani, W.-G. Shim, M.-J. Lee, C. Kim, J.-W. Lee, H. Moon, Highly porous electrodes from novel corn grains-based activated carbons for electrical double layer capacitors, Electrochem. Commun. 10 (2008) 868–871.
[14] H. Chen, H. Wang, L. Yang, Y. Xiao, High specific surface area rice hull based porous carbon prepared for EDLCs, Int. J. Electrochem. Sci. 7 (2012) 4889–4897.
[15] L. Hao, X. Li, L. Zhi, Carbonaceous electrode materials for supercapacitors, Adv. Mater. 25 (2013) 3899–3904.
[16] M. Inagaki, H. Konno, O. Tanaike, Carbon materials for electrochemical capacitors, J. Power Sources 195 (2010) 7880–7903.
[17] K. Kierzek, E. Frackowiak, G. Lota, G. Gryglewicz, J. Machnikowski, Electrochemical capacitors based on highly porous carbons prepared by KOH activation, Electrochim. Acta 49 (2004) 515–523.
[18] M. Sevilla, A.B. Fuertes, Direct synthesis of highly porous interconnected carbon nanosheets and their application as high-performance supercapacitors, ACS Nano 8 (2014) 5069–5078.
[19] J. Wang, S. Kaskel, KOH activation of carbon-based materials for energy storage, J. Mater. Chem. 22 (2012) 23710.
[20] L. Wei, M. Sevilla, A.B. Fuertes, R. Mokaya, G. Yushin, Polypyrrole-derived activated carbons for high-performance electrical double-layer capacitors with ionic liquid electrolyte, Adv. Funct. Mater. 22 (2012) 827–834.
[21] C. Zhang, X. Zhu, M. Cao, M. Li, N. Li, L. Lai, J. Zhu, D. Wei, Hierarchical porous carbon materials derived from sheep manure for high-capacity supercapacitors, ChemSusChem 9 (2016) 932–937.
[22] G. Zhang, L. Wang, Y. Hao, X. Jin, Y. Xu, Y. Kuang, L. Dai, X. Sun, Unconventional carbon: alkaline dehalogenation of polymers yields n-doped carbon electrode for high-performance capacitive energy storage, Adv. Funct. Mater. 26 (2016) 3340–3348.
[23] J. Chmiola, C. Largeot, P.-L. Taberna, P. Simon, Y. Gogotsi, Desolvation of ions in subnanometer pores and its effect on capacitance and double-layer theory, Angew. Chem. 120 (2008) 3440–3443.
[24] J. Chmiola, G. Yushin, Y. Gogotsi, C. Portet, P. Simon, P.L. Taberna, Anomalous increase in carbon capacitance at pore sizes less than 1 nanometer, Science 313 (2006) 1760–1763.
[25] Y. Gogotsi, A. Nikitin, H. Ye, W. Zhou, J.E. Fischer, B. Yi, H.C. Foley, M.W. Barsoum, Nanoporous carbide-derived carbon with tunable pore size, Nat. Mater. 2 (2003) 591–594.
[26] J. Huang, B.G. Sumpter, V. Meunier, A universal model for nanoporous carbon supercapacitors applicable to diverse pore regimes, carbon materials, and electrolytes, Chem. Eur. J. 14 (2008) 6614–6626.
[27] D.-e. Jiang, Z. Jin, D. Henderson, J. Wu, Solvent effect on the pore-size dependence of an organic electrolyte supercapacitor, J. Phys. Chem. Lett. 3 (2012) 1727–1731.
[28] D.-e. Jiang, Z. Jin, J. Wu, Oscillation of capacitance inside nanopores, Nano Lett. 11 (2011) 5373–5377.
[29] D.-e. Jiang, J. Wu, Unusual effects of solvent polarity on capacitance for organic electrolytes in a nanoporous electrode, Nanoscale 6 (2014) 5545–5550.
[30] C. Largeot, C. Portet, J. Chmiola, P.-L. Taberna, Y. Gogotsi, P. Simon, Relation between the ion size and pore size for an electric double-layer capacitor, J. Am. Chem. Soc. 130 (2008) 2730–2731.
[31] T. Ohba, K. Kaneko, Competition of desolvation and stabilization of organic electrolytes in extremely narrow nanopores, J. Phys. Chem. C 117 (2013) 17092–17098.
[32] F. Stoeckli, T.A. Centeno, Pore size distribution and capacitance in microporous carbons, Phys. Chem. Chem. Phys. 14 (2012) 11589–11591.
[33] Y. Li, Z. Li, P.K. Shen, Simultaneous formation of ultrahigh surface area and three-dimensional hierarchical porous graphene-like networks for fast and highly stable supercapacitors, Adv. Mater. 25 (2013) 2474–2480.
[34] Y. Zhu, S. Murali, M.D. Stoller, K.J. Ganesh, W. Cai, P.J. Ferreira, A. Pirkle, R.M. Wallace, K.A. Cychosz, M. Thommes, D. Su, E.A. Stach, R.S. Ruoff, Carbon-based supercapacitors produced by activation of graphene, Science 332 (2011) 1537–1541.
[35] L. Estevez, R. Dua, N. Bhandari, A. Ramanujapuram, P. Wang, E.P. Giannelis, A facile approach for the synthesis of monolithic hierarchical porous carbons - high performance materials for amine based $CO_2$ capture and supercapacitor electrode, Energy Environ. Sci. 6 (2013) 1785–1790.
[36] T. Lin, I.-W. Chen, F. Liu, C. Yang, H. Bi, F. Xu, F. Huang, Nitrogen-doped mesoporous carbon of extraordinary capacitance for electrochemical energy storage, Science 350 (2015) 1508–1513.
[37] G. Yushin, R. Dash, J. Jagiello, J.E. Fischer, Y. Gogotsi, Carbide-derived carbons: effect of pore size on hydrogen uptake and heat of adsorption, Adv. Funct. Mater. 16 (2006) 2288–2293.
[38] R. Pena-Alonso, G.D. Soraru, R. Raj, Preparation of ultrathin-walled carbon-based nanoporous structures by etching pseudo-amorphous silicon oxycarbide ceramics, J. Am. Ceram. Soc. 89 (2006) 2473–2480.
[39] A. Saha, R. Raj, D.L. Williamson, A model for the nanodomains in polymer-derived SiCO, J. Am. Ceram. Soc. 89 (2006) 2188–2195.
[40] A. Meier, M. Weinberger, K. Pinkert, M. Oschatz, S. Paasch, L. Giebeler, H. Althues, E. Brunner, J. Eckert, S. Kaskel, Silicon oxycarbide-derived carbons from a polyphenylsilsequioxane precursor for supercapacitor applications, Microporous Mesoporous Mater. 188 (2014) 140–148.
[41] C. Vakifahmetoglu, V. Presser, S.-H. Yeon, P. Colombo, Y. Gogotsi, Enhanced hydrogen and methane gas storage of silicon oxycarbide derived carbon, Microporous Mesoporous Mater. 144 (2011) 105–112.
[42] H. Wu, J. Yang, H. Chen, F. Pan, Revealing the nanodomain structure of silicon oxycarbide via preferential etching and pore analysis, Funct. Mater. Lett. 09 (2016) 1650043.
[43] Y. Guo, S. Yang, K. Yu, J. Zhao, Z. Wang, H. Xu, The preparation and mechanism studies of rice husk based porous carbon, Mater. Chem. Phys. 74 (2002) 320–323.
[44] J.C.C. Freitas, M.A. Schettino, A.G. Cunha, F.G. Emmerich, A.C. Bloise, E.R. de Azevedo, T.J. Bonagamba, NMR investigation on the occurrence of Na species in porous carbons prepared by NaOH activation, Carbon 45 (2007) 1097–1104.
[45] M.A. Lillo-Ródenas, D. Cazorla-Amorós, A. Linares-Solano, Understanding chemical reactions between carbons and NaOH and KOH, Carbon 41 (2003) 267–275.
[46] M.A. Lillo-Ródenas, J. Juan-Juan, D. Cazorla-Amorós, A. Linares-Solano, About reactions occurring during chemical activation with hydroxides, Carbon 42 (2004) 1371–1375.
[47] A.C. Ferrari, J. Robertson, Interpretation of Raman spectra of disordered and amorphous carbon, Phys. Rev. B 61 (2000) 14095–14107.
[48] F. Tuinstra, Raman spectrum of graphite, J. Chem. Phys. 53 (1970) 1126.
[49] T.I.T. Okpalugo, P. Papakonstantinou, H. Murphy, J. McLaughlin, N.M.D. Brown, High resolution XPS characterization of chemical functionalised MWCNTs and SWCNTs, Carbon 43 (2005) 153–161.
[50] Y.S. Yun, S. Lee, N.R. Kim, M. Kang, C. Leal, K.-Y. Park, K. Kang, H.-J. Jin, High and rapid alkali cation storage in ultramicroporous carbonaceous materials, J. Power Sources 313 (2016) 142–151.
[51] Y. Li, Y. Zhao, H. Cheng, Y. Hu, G. Shi, L. Dai, L. Qu, Nitrogen-doped graphene quantum dots with oxygen-rich functional groups, J. Am. Chem. Soc. 134 (2012) 15–18.
[52] H. Luo, Y. Yang, B. Mu, Y. Chen, J. Zhang, X. Zhao, Facile synthesis of microporous carbon for supercapacitors with a LiNO3 electrolyte, Carbon 100 (2016) 214–222.
[53] V. Datsyuk, M. Kalyva, K. Papagelis, J. Parthenios, D. Tasis, A. Siokou, I. Kallitsis, C. Galiotis, Chemical oxidation of multiwalled carbon nanotubes, Carbon 46 (2008) 833–840.
[54] P. Cheng, T. Li, H. Yu, L. Zhi, Z. Liu, Z. Lei, Biomass-derived carbon fiber aerogel as a binder-free electrode for high-rate supercapacitors, J. Phys. Chem. C 120 (2016) 2079–2086.
[55] W. Tian, Q. Gao, Y. Tan, K. Yang, L. Zhu, C. Yang, H. Zhang, Bio-inspired beehive-like hierarchical nanoporous carbon derived from bamboo-based industrial by-product as a high performance supercapacitor electrode material, J. Mater. Chem. A 3 (2015) 5656–5664.
[56] J. Hao, Y. Liao, Y. Zhong, D. Shu, C. He, S. Guo, Y. Huang, J. Zhong, L. Hu, Three-dimensional graphene layers prepared by a gas-foaming method for supercapacitor applications, Carbon 94 (2015) 879–887.
[57] L. Qie, W. Chen, H. Xu, X. Xiong, Y. Jiang, F. Zou, X. Hu, Y. Xin, Z. Zhang, Y. Huang, Synthesis of functionalized 3D hierarchical porous carbon for high-performance supercapacitors, Energy Environ. Sci. 6 (2013) 2497–2504.
[58] S.J. Yang, T. Kim, J.H. Im, Y.S. Kim, K. Lee, H. Jung, C.R. Park, MOF-derived hierarchically porous carbon with exceptional porosity and hydrogen storage capacity, Chem. Mater. 24 (2012) 464–470.
[59] S. Bai, G. Tan, X. Li, Q. Zhao, Y. Meng, Y. Wang, Y. Zhang, D. Xiao, Pumpkin-derived porous carbon for supercapacitors with high performance, Chem. Asian J. 11 (2016) 1828–1836.
[60] A. Bello, N. Manyala, F. Barzegar, A.A. Khaleed, D.Y. Momodu, J.K. Dangbegnon, Renewable pine cone biomass derived carbon materials for supercapacitor application, RSC Adv. 6 (2016) 1800–1809.
[61] P. Cheng, S. Gao, P. Zang, X. Yang, Y. Bai, H. Xu, Z. Liu, Z. Lei, Hierarchically porous carbon by activation of shiitake mushroom for capacitive energy storage, Carbon 93 (2015) 315–324.

[62] Q. Li, R. Jiang, Y. Dou, Z. Wu, T. Huang, D. Feng, J. Yang, A. Yu, D. Zhao, Synthesis of mesoporous carbon spheres with a hierarchical pore structure for the electrochemical double-layer capacitor, Carbon 49 (2011) 1248–1257.
[63] Y. Li, G. Wang, T. Wei, Z. Fan, P. Yan, Nitrogen and sulfur co-doped porous carbon nanosheets derived from willow catkin for supercapacitors, Nano Energy 19 (2016) 165–175.
[64] Q. Liang, L. Ye, Z.-H. Huang, Q. Xu, Y. Bai, F. Kang, Q.-H. Yang, A honeycomb-like porous carbon derived from pomelo peel for use in high-performance supercapacitors, Nanoscale 6 (2014) 13831–13837.
[65] Y. Liang, F. Liang, H. Zhong, Z. Li, R. Fu, D. Wu, An advanced carbonaceous porous network for high-performance organic electrolyte supercapacitors, J. Mater. Chem. A 1 (2013) 7000.
[66] C. Long, X. Chen, L. Jiang, L. Zhi, Z. Fan, Porous layer-stacking carbon derived from in-built template in biomass for high volumetric performance supercapacitors, Nano Energy 12 (2015) 141–151.
[67] D. Puthusseri, V. Aravindan, S. Madhavi, S. Ogale, 3D micro-porous conducting carbon beehive by single step polymer carbonization for high performance supercapacitors: the magic of in situ porogen formation, Energy Environ. Sci. 7 (2014) 728–735.
[68] W. Sun, S.M. Lipka, C. Swartz, D. Williams, F. Yang, Hemp-derived activated carbons for supercapacitors, Carbon 103 (2016) 181–192.
[69] K. Wang, Y. Cao, X. Wang, Q. Fan, W. Gibbons, T. Johnson, B. Luo, Z. Gu, Pyrolytic cyanobacteria derived activated carbon as high performance electrode in symmetric supercapacitor, Energy 94 (2016) 666–671.
[70] Q. Xie, A. Zheng, S. Zhai, S. Wu, C. Xie, Y. Zhang, Y. Guan, Reed straw derived active carbon/graphene hybrids as sustainable high-performance electrodes for advanced supercapacitors, J. Solid State Electrochem. 20 (2016) 449–457.
[71] A.J. Pak, G.S. Hwang, Charging rate dependence of ion migration and stagnation in ionic-liquid-filled carbon nanopores, J. Phys. Chem. C 120 (2016) 24560–24567.

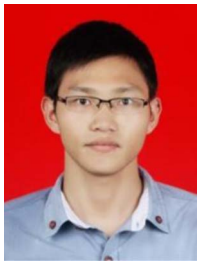

**Jie Yang** received his Bachelor's degree in materials science and engineering from Hainan University, China, in 2014. He is pursuing his master's degree in the School of Advanced Materials, Peking University, China. His main research interests include advanced carbon materials for energy storage and conversion such as supercapacitors, lithium ion batteries and metal-air batteries.

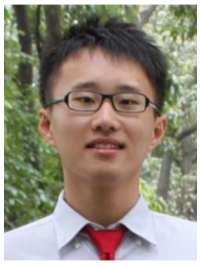

**Haolin Wu** received his Bachelor's degree from South China University of Technology, China, in 2014. He received his Master's degree from Peking University, Shenzhen Graduate School. He was working on developing ceramics and carbon materials for supercapacitors and lithium ion batteries. Currently he is an employee of the China Development Bank.

**Min Zhu** received his Bachelor's degree (BE) in 2015 from Tsinghua University. He is currently a master student major in materials chemistry in Peking University Shenzhen Graduate School. His research is mainly focused on porous materials and anode materials for lithium ion batteries.

**Wenju Ren** received his Master's degree in 2008 from Yanshan University, China. He is currently a PhD student in Peking University Shenzhen Graduate School. His research is mainly focused on synthesizing nanomaterials and studying their properties for LIBs.

**Prof. Yuan Lin**, Institute of Chemistry, Chinese academy of Sciences, got B.S. from Dept. Chemistry, Peking University in1985, M.S and Ph.D. from Chinese Academy of Sciences (CAS) in 1988 and 1995, respectively. In 1988–1999, he took the position of assistant professor at Institute of Photographic Chemistry, Chinese Academy of Sciences. From 1999 to present, he took the position of full professor. For more than 20 years, Prof. Lin has been engaged in the fields of photoelectrochemical conversion of solar energy, preparation of nanocrystalline semiconductors, investigation of photoelectrochemical and surface properties of nanocrystalline semiconductors, developing ionic liquid and polymeric materials for electrolytes.

**Haibiao Chen** is currently a senior researcher at the School of Advanced Materials, Peking University Shenzhen Graduate School. He received his Bachelor's degree from Tsinghua University in 2000 and Ph.D. from Stevens Institute of Technology in 2006. He worked at Velocys during 2006–2011 and UES during 2011–2014 prior to joining Peking University Shenzhen Graduate School.

**Prof. Feng Pan**, National 1000-plan Professor, Founding Dean of School of Advanced Materials, Peking University Shenzhen Graduate School, Director of National Center of Electric Vehicle Power Battery and Materials for International Research, got B.S. from Dept. Chemistry, Peking University in1985 and PhD from Dept. of P&A Chemistry, University of Strathclyde, Glasgow, UK, with "Patrick D. Ritchie Prize" for the best Ph.D. in 1994. With more than a decade experience in large international incorporations, Prof. Pan has been engaged in fundamental research and product development of novel optoelectronic and energy storage materials and devices. As Chief Scientist, Prof. Pan led 8 entities in Shenzhen to win the 150 million RMB grant for the national new energy vehicles (power battery) innovation project from 2013 to end of 2015. As Chief Scientist, Prof. Pan led 12 entities to win National Key project of Material Genomic Engineering for Solid State Li-ion Battery in China in 2016.